Journal of Ceramic Processing Research. Vol. 14, No. 1, pp. 59~64 (2013)

J O U R N A L O F
Ceramic Processing Research

Characterization of $Ni_{1-x}Cu_x$-$Ce_{0.8}Gd_{0.2}O_{1.9}$ composite anodes for methane-fueled solid oxide fuel cells

Chun-Kang Cho[a] and Ki-Tae Lee[a,b,c,*]

[a]*Department of Hydrogen Fuel Cells Engineering, Specialized Graduate School, Chonbuk National University, Jeonbuk 561-756, Korea*
[b]*Division of Advanced Materials Engineering, Chonbuk National University, Jeonbuk 561-756, Korea*
[c]*Hydrogen and Fuel Cells Research Center, Chonbuk National University, Jeonbuk 561-756, Korea*

$Ni_{1-x}Cu_x$-$Ce_{0.8}Gd_{0.2}O_{1.9}$ cermet anodes were co-synthesized by a glycine nitrate process (GNP). While the polarization resistance in an H_2 atmosphere increased with increasing Cu content, both electrical conductivity and the amount of carbon deposits were reduced by Cu alloying. The anode polarization resistance in CH_4 fuel decreased with increasing Cu content, which strongly correlates with the carbon deposition behavior. Cu doping significantly improved the electrochemical performance in CH_4 fuel.

Key words: Solid oxide fuel cell, Composite anode, Ni-Cu alloy, Carbon deposition.

Introduction

A solid oxide fuel cell (SOFC) consists entirely of solid state material, including the electrolytes. In order to obtain high ionic conductivity with solid electrolytes, the operating temperature must be very high [1-3]. However, the high operating temperature allows the use of a variety of fuels in SOFCs, and improves the conversion efficiency by up to 70% with a combined heat and generation system [4].

Nickel is the most commonly used anode material, because it is inexpensive, and meets the requirements for a SOFC anode. Nickel provides high catalytic activity for the oxidation of H_2 in SOFCs [5]. Usually, nickel is used with yttria stabilized zirconia (YSZ) as a ceramic-metallic composite (cermet). YSZ in the Ni-YSZ cermet plays the important roles of matching the thermal expansion with other components, suppressing grain growth of Ni, and providing ionic conductivity. For Ni-YSZ anode materials, however, there are some disadvantages, such as a low tolerance of sulfur, poor redox stability, and the agglomeration of nickel after long-term operation [6-8]. In particular, when carbon deposition occurs during internal reforming, the active sites of the Ni anode are covered by the deposited carbon, which results in a degradation of the catalytic activity, a decrease of the cell performance, and a low reliability [9, 10]. In order to overcome the carbon deposition problem, many researchers are focusing on finding novel or alternative SOFC anode materials, such as metal-ceramic composites, nickel alloys, ceria based and perovskite structured oxides.

*Corresponding author:
Tel : +82-63-270-2290
Fax: +82-63-270-2386
E-mail: ktlee71@jbnu.ac.kr

Ni in the Ni-YSZ cermet anode can be replaced partly or completely by other metals, such as Co or Cu, to improve the tolerance for carbon deposition. It has been reported that Cu could avoid carbon deposition when using hydrocarbon fuel [11, 12]. Compared to Ni, however, Cu shows poorer catalytic activity. Meanwhile, ceria (CeO_2) can provide a high catalytic activity for hydrocarbon reforming, due to its mixed ionic-electronic conductivity [13]. In particular, Gd or Sm doped ceria shows much higher ionic conductivity than YSZ at low temperatures.

In this regard, Ni-Cu alloys with $Ce_{0.8}Gd_{0.2}O_{1.9}$ (GDC) as alternative anode materials have been selected and investigated in this study. The effects of Cu on the crystal chemistry, electrical conductivity, carbon deposition, and electrochemical performance have been investigated.

Experimental procedure

$Ni_{1-x}Cu_xO$-GDC powders were synthesized by a glycine nitrate process (GNP). The synthesized compositions and their abbreviations are listed in Table 1. $Ni(NO_3)_26H_2O$ (Alfa Aesar, 98%), $Cu(NO_3)_25H_2O$ (Alfa Aesar, 98%), $Ce(NO_3)_36H_2O$ (Aldrich, 99% metal basis), $Gd(NO_3)_36H_2O$ (Alfa Aesar, 99.9%, REO), and glycine (Alfa Aesar, 99%) were dissolved into dionized water. After stirring for 2 h, the mixed solution was heated at about 250 °C until combustion occurred. The ashes formed by the combustion were calcined at 750 °C for 2 h, followed by ball-milling for 24 h. For the re-dox stability test, the calcined samples were further reduced in a H_2 atmosphere at 800 °C for 2 h.

Powder X-ray diffraction analysis was conducted using a X-ray diffractometer (Rigaku Model D/MAX-111A, Japan) with Cu Kα radiation to analyze phases, the solubility limit, and redox stability. Diffraction

Table 1. Compositions synthesized and abbreviations of the $Ni_{1-x}Cu_x$-GDC composite anode materials.

Composition	Abbreviation
Ni-$Ce_{0.8}Gd_{0.2}O_{1.9}$	Ni-GDC
$Ni_{0.95}Cu_{0.05}$-$Ce_{0.8}Gd_{0.2}O_{1.9}$	Cu05
$Ni_{0.9}Cu_{0.1}$-$Ce_{0.8}Gd_{0.2}O_{1.9}$	Cu10
$Ni_{0.85}Cu_{0.15}$-$Ce_{0.8}Gd_{0.2}O_{1.9}$	Cu15

*$Ni_{1-x}Cu_x$: $Ce_{0.8}Gd_{0.2}O_{1.9}$ = 60 vol.% : 40 vol.%

patterns were recorded with a scan rate of 4 °·min^{-1} in the 2θ range of 20 ° to 80 °. Lattice constants were calculated from the XRD results. For the microstructural analysis and electrical conductivity measurement, bar-type samples were sintered at 1400 °C for 4 h in an air atmosphere. The porosity of the sintered samples was measured by the Archimedes method. The confirmation of the microstructures and compositions was conducted by a scanning electron microscopy/energy-dispersive X-ray spectroscopy (SEM/EDX, SN-3000 Hitachi, Japan). Electrical conductivity of the sintered samples was measured by the DC 4-probe method. The amount of carbon deposition was calculated by thermal gravimetric analysis (TGA, TA Q600, TA instruments Ltd., USA). While the calcined samples were exposed in a dry CH_4 atmosphere at 800 °C for 3 h, the carbon decomposed from CH_4 was deposited on the surface of samples. TGA was carried out from room temperature to 900 °C with a heating rate of 20 °C·min^{-1} in air. By conducting TGA with the samples in air, the carbon is re-oxidized with oxygen. Thus, the amount of the deposited carbon can be calculated by analyzing the weight loss from 500 °C to 700 °C.

Symmetric cells with 8 mol.% yttria stabilized zirconia (8YSZ) electrolyte were fabricated for the electrochemical characterization. 8YSZ pellets were sintered with commercial YSZ powder (TZ-8YSZ, Tosoh, Japan) at 1450 °C for 4 h. The anode paste was made by mixing the anode powders and binder (Heraeus V006) in a ratio of 70 : 30 wt.%, and the paste was screen-printed on both sides of theYSZ pellets to make electrodes of 0.25 cm^2 geometrical area. Afterwards, both electrodes were fired at the proper temperature and time. Pt mesh and Pt wire were used as a current collector and a lead, respectively. The AC impedance analysis of the samples prepared was conducted with a potentiostat (SP150, Biologic SAS, France), having a frequency response analyzer under open-circuit conditions at 800 °C in both H_2 and CH_4 atmospheres. The range of the applied frequency was from 50 μHz to 100 kHz with a voltage amplitude of 20 mV.

Results and Discussion

X-ray diffraction patterns of the $Ni_{1-x}Cu_xO$ powders with various Cu contents (x = 0.05 ~ 0.7) are shown in Fig. 1. No secondary peaks were detected below x = 0.15. When a higher amount of Cu was added in NiO, the peaks of CuO were observed. The solubility limit of Cu in NiO was considered to bebelow 15 mol.%. The calcined powders were reduced in a H_2 atmosphere at 800 °C for 2 h, in order to identify the solubility limit at the metal state of $Ni_{1-x}Cu_x$. X-ray diffraction patterns and the variation of lattice constants of the $Ni_{1-x}Cu_x$ powders with various Cu contents (x = 0, 0.25, 0.5, 0.75) are shown in Fig. 2. Unlike $Ni_{1-x}Cu_xO$, Cu was completely alloyed in the Ni, and there were no impurities, even at a high amount of Cu

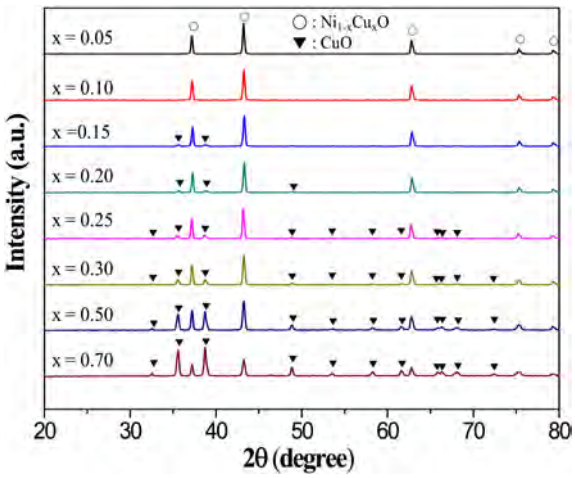

Fig. 1. XRD patterns of $Ni_{1-x}Cu_xO$ with various dopant contents, calcined in an air atmosphere at 750 °C for 2 h.

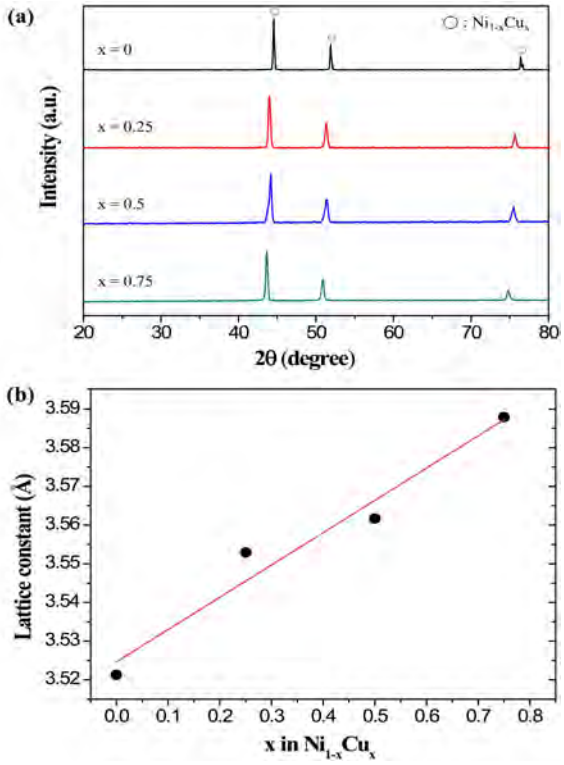

Fig. 2. (a) XRD patterns and (b) lattice constants of $Ni_{1-x}Cu_x$ with various dopant contents, reduced in H_2 at 800 °C for 2 h.

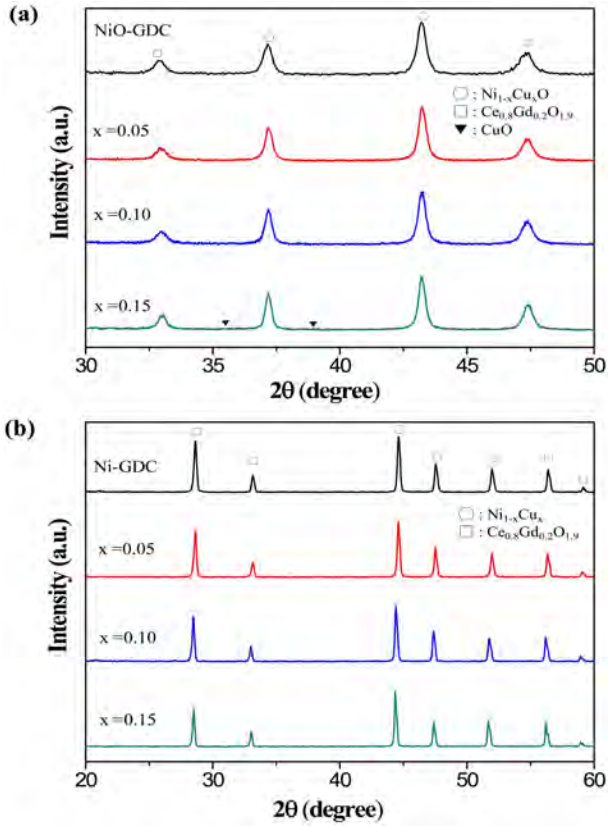

Fig. 3. XRD patterns of the $Ni_{1-x}Cu_xO$-GDC composites (a) calcined in air at 750 °C for 2 h and (b) reduced in H_2 at 800 °C for 2 h.

Table 2. EDX elemental analysis data and porosity for the reduced samples after sintering at 1400 °C for 4 h in air.

Composition	Stoichiometry of elements (%)				Porosity (%)
	Ni	Cu	Ce	Gd	
Ni-GDC	100	0	79.43	20.57	31
Cu05	94.99	5.01	80.25	19.75	38
Cu10	90.76	9.24	80.32	19.68	45
Cu15	85.97	14.05	81.09	18.91	49

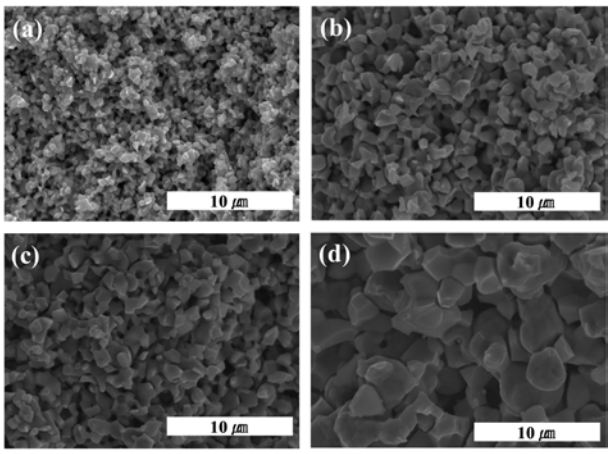

Fig. 4. Cross-sectional SEM micrographs of the $Ni_{1-x}Cu_x$-GDC composites reduced in H_2 at 800 °C for 2 h after sintering at 1400 °C for 4 h in air: (a) x = 0, (b) x = 0.05 (c) x = 0.1 (d) x = 0.15.

doping. Cu was completely solid-soluble in Ni. The peaks of $Ni_{1-x}Cu_x$ shifted in the direction of a low 2θ with increasing Cu contents. This indicates typical lattice substitution, and is mainly due to the difference of atomic radius between Ni (R_{Ni} = 1.24 Å) and Cu (R_{Cu} = 1.28 Å) [14]. The variations of the lattice constant of $Ni_{1-x}Cu_x$ were linear with increasing dopant contents, and meet Vegard's law very well [15].

$Ni_{1-x}Cu_xO$-GDC powders were also co-synthesized by GNP for a composite anode application. X-ray diffraction patterns of the $Ni_{1-x}Cu_xO$-GDC composite powders co-synthesized by GNP after being calcined in air at 750 °C for 2 h are shown in Fig. 3(a). Although there were no reaction products between $Ni_{1-x}Cu_xO$ and GDC, CuO peaks were detected at x = 0.15. This accords well with the solubility limit analysis of $Ni_{1-x}Cu_xO$, as shown in Fig. 1. However, when the calcined $Ni_{1-x}Cu_xO$-GDC powders were reduced in a H_2 atmosphere at 800 °C for 2 h, Cu was completely alloyed in the Ni lattice in $Ni_{1-x}Cu_x$-GDC composites without any reaction products, as shown in Fig. 3(b). This result also shows the same trend with the XRD results of the reduced $Ni_{1-x}Cu_x$ synthesized without GDC, as shown in Fig. 2.

In order to verify the compositions as designed, quantitative analysis was carried out by EDX, and the results are given in Table 2. From elemental analysis, it can be confirmed that the synthesized samples as designed were well formed in stoichiometry.

The microstructures and the measured porosity of the reduced samples after sintering at 1400 °C for 4 h in air are shown in Fig. 4 and Table 2, respectively. Increasing the Cu content resulted in an increase of grain size. This grain growth with Cu alloying is due to the low melting point of Cu (1083 °C). Although no pore formers were used, all samples had sufficient porosity, over 30%, to allow gas permeation. The porosity increased with increasing Cu content, as shown in Table 2.

The electrical conductivities of the $Ni_{1-x}Cu_x$-GDC samples measured by the DC 4-probe method are shown in Fig. 5. The electrical conductivity of the samples decreased with increasing Cu content. This is attributed to both the microstructure and electronic structure. As shown in Table 2, the porosity increases with the Cu content, which leads to a disconnection between particles. It has also been reported that the resistivity of a Ni-Cu alloy with a higher concentration range of Ni increased with the Cu content, which means the electrical conductivity decreases with Cu addition [16]. These electrical behaviors of the Ni-Cu alloy system are due to the enhancement of electron scattering by the solid solution effect, based on Nordheim's rule. However, the main point is that all of the alloyed samples with a porous structure still showed high conductivity above 1800 S/cm at 800 °C in a H_2 atmosphere,

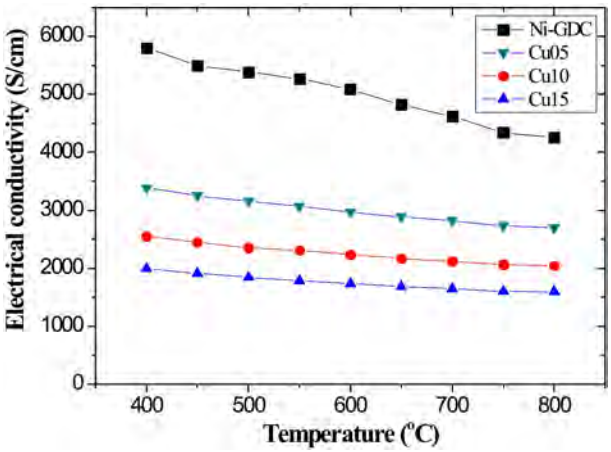

Fig. 5. Electrical conductivity of the $Ni_{1-x}Cu_x$-GDC composites measured in a reducing atmosphere.

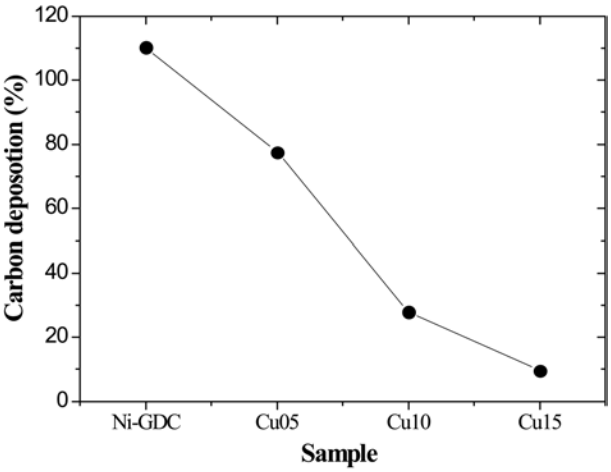

Fig. 6. Carbon deposition rate of the $Ni_{1-x}Cu_x$-GDC composites with various dopant contents.

which can meet the requirement of SOFC anodes.

The calculated carbon deposition rates of all the samples from the TGA data are shown in Fig. 6. The amount of carbon deposits for the Cu-alloyed samples was reduced, compared with that for Ni-GDC. The carbon deposition rate gradually decreased with an increase of the Cu content. In the CH_4 fueled-SOFC system, CH_4 is internally reformed by a steam reforming process (Eq. 1) or a partial oxidation reaction (Eq. 2):

$$CH_4+H_2O\rightarrow CO+3H_2 \quad (1)$$

$$CH_4+O^{2-}\rightarrow CO+2H_2+2e^- \quad (2)$$

However, part of the CH_4 can be decomposed and deposited on the anode surface. The formation of carbon at the CH_4 fueled-SOFC anode generally occurs via pyrolysis (Eq. 3) or the Boudouard reaction (Eq. 4):

$$CH_4\rightarrow C+2H_2 \quad (3)$$

$$2CO\rightarrow CO_2+C \quad (4)$$

Since in this research the carbon deposition behavior was evaluated in a dry CH_4 atmosphere, CH_4 pyrolysis is considered as a dominant mechanism for the carbon deposition. Ni is well known as a simple catalyst for the formation of both carbon filaments and nickel carbide from the cracked carbon species on its surface [17, 18]. On the other hand, Cu is thought to be noncatlytic to carbon deposition from gas atmospheres, due to its extremely low solubility for carbon [19]. Galea et al. have shown that the thermodynamic and kinetic barriers to CH_4 dissociation are very high on

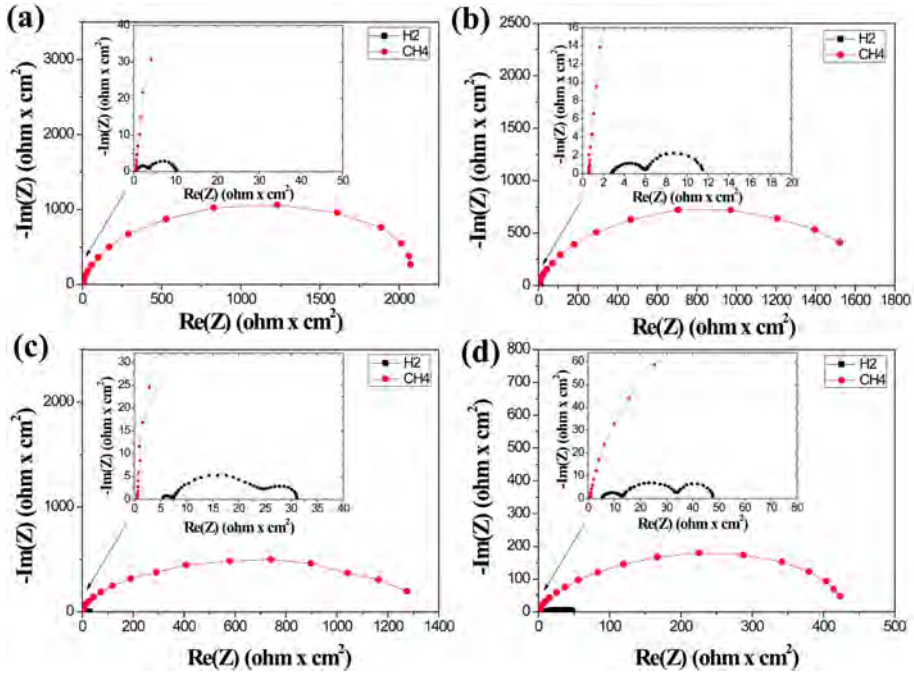

Fig. 7. Typical AC impedance spectra of the symmetrical half cells with $Ni_{1-x}Cu_x$-GDC anodes and YSZ electrolyte in H_2 and CH_4 at 800 °C.

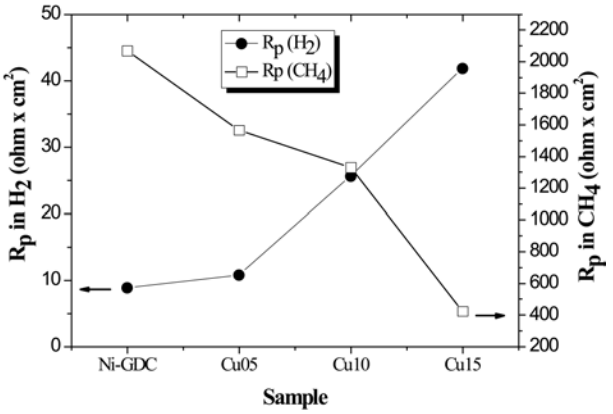

Fig. 8. Variation of R_p values of the $Ni_{1-x}Cu_x$-GDC composites with various dopant contents in H_2 and CH_4 at 800 °C.

both the Cu (111) planar and Cu (211) stepped surfaces, and the resistance to coking for the Cu-Ni alloy is due to Cu enrichment of the alloy surface and/or blocking of the active step sites [20]. Similarly, Nikolla et al. have reported that the surface chemistry of Ni can be changed significantly by doping small amounts of Sn to form Sn-Ni alloys [21]. The Sn modified-surface of alloy can suppress the formation of C-C bonds and/or can have a lower thermodynamic driving force for carbon nucleation on the low-coordinated sites [22]. Thus Cu alloying in a Ni matrix may inhibit the formation of carbon deposits, by breaking up ensembles of Ni atoms, as well as by providing thermodynamic and kinetic barriers to CH_4 dissociation.

The typical AC impedance spectra of the symmetrical half cells with an YSZ electrolyte at 800 °C are shown in Fig. 7. The left intercept with the impedance arc on the Z (real) axis at high frequencies corresponds to the Ohmic resistance, R_o, and the right intercept on the Z (real) axis indicates total resistance, R_{tot}. The polarization resistance, R_p, is the overall size of the arcs (R_{tot}-R_o). Considering the oxidation of H_2 via a CH_4 reforming process, it can readily be expected that H_2 fueled SOFC shows better performance than a CH_4 fueled SOFC. The anode polarization resistance for CH_4 fuel is much larger than that for H_2 fuel, due to a surface reaction. This is also partly because pore diffusion of CH_4 molecules is more difficult than that of H_2 molecules, due to the size effect.

Variations of R_p values in both an H_2 and a CH_4 atmosphere are shown in Fig. 8. The R_p value in H_2 increased with increasing dopant contents. This is due to a decrease in catalytic activity, and in electrical conductivity by doping, as shown in Fig. 5. The anode reaction on a SOFC is generally considered as a multiphase reaction including catalytic activation, the adsorption/dissociation of the hydrogen molecule, charge transfer, and gas diffusion. The electronic conductivity of the anode material is one of the critical parameters for maximizing the electrochemical performance. The electronic conductivity is strongly related to a charge transfer reaction. A lower electrical conductivity inhibits the charge transfer reaction, due to the lack of electrons supplied. In addition to electronic conductivity, the number of reaction sites, such as triple phase boundaries (TPB, anode/electrolyte/gas), is also an important factor. As shown in Fig. 4, the grain size increases with increasing Cu content, which results in a decrease in the amount of TPB. Consequently, the electrochemical performance in H_2 degrades with Cu alloying, due to decrease in both the electrical conductivity and the number of reaction sites. On the other hand, the R_p values in CH_4 decreased with increasing Cu content. It has been reported that the high-frequency arc in the AC impedance data is generally related to the electrode microstructure of the anode and gas diffusion [23]. Therefore, the limitation to gas diffusion of the $Ni_{1-x}Cu_x$-GDC samples in CH_4 might be caused by carbon deposits, which subsequently blocked the anode pores. Moreover, the carbon deposits may cover the reaction sites.This leads to suppression of the catalytic activity. The variation of the R_p value in CH_4 shows the same trend as that of the carbon deposition rate, as shown in Fig. 6. Consequently, Cu alloying could reduce the carbon deposition rate, resulting in an electrochemical performance improvement for the CH_4 fuel.

Conclusions

Ni-Cu alloy based anode materials have been investigated from a perspective of the development of alternative SOFC anode materials for hydrocarbon fuel use. Although there was a solubility limit of Cu in NiO, all dopants were completely alloyed in Ni metal in a reduced atmosphere.

Both the electrical conductivity and the carbon deposition rate of the $Ni_{1-x}Cu_x$-GDC composite decreased with increasing Cu content. The electrical conductivity of the composite decreased due to the electron scattering effect in a solid solution; while the carbon deposition rate decreased due to a suppression of the formation of C-C bonds and/or a lowering of the thermodynamic driving force for carbon nucleation.

The anode polarization resistance in a CH_4 atmosphere decreased with an increase of the dopant contents. Consequently, Cu alloying was effective at suppressing carbon deposition and improving the electrochemical performance of solid oxide fuel cells in CH_4 fuel.

Acknowledgements

This research was supported by the Basic Science Research Program through the National Research Foundation of Korea (NRF) funded by the Ministry of Education, Science and Technology (Grant No. 2010-0009130). This work was also supported by the Human Resources Development of the Korea Institute of

Energy Technology Evaluation and Planning (KETEP) funded by the Korea government Ministry of Knowledge Economy (Grant No. 20114030200060).

References

1. S.P. Jiang, S.H. Chan, J. Mater. Sci. 39 (2004) 4405-4439.
2. W.Z. Zhu, S.C. Deevi, Mater. Sci.Eng. A 362 (2003) 228-239.
3. A.L. Sauvet, J. Fouletier, J. Power Sources 101 (2001) 259-266.
4. K. Eguchi, Y. Kunisa, K. Adachi, H. Arai, J. Electrochem. Soc.143 (1996) 3699-3703.
5. S.P. Jiang, S.H. Chan, Mater. Sci. Technol. 20 (2004) 1109-1118.
6. B.C.H. Steel, Solid State Ionics 86-88 (1996) 1223-1234.
7. C.H. Bartholomew, Catal. Rev. Sci. Eng. 24 (1982) 67-70.
8. K. Hernadi, A. Fonseca, J.B. Nagy, A. Siska, I. Kiricsi, Appl. Catal. A199 (2000) 245-255.
9. T. Takeguchi, Y. Kani, T. Yano, R. Kikuchi, K. Eguchi, K. Tsujimoto, Y. Uchida, A. Ueno, K. Omoshiki, M. Aizawa, J. Power Sources, 112 (2002) 588-595.
10. A.L. Dicks, J. Power Sources, 61 (1996) 113-124.
11. R.J. Gorte, S. Park, J.M. Vohs, C. Wang, Adv. Mater. 12 (2000) 1465-1469.
12. S. Park, R. Craciun, J.M. Vohs, R.J. Gorte, J. Electrochem. Soc. 146 (1999) 3603-3605.
13. A. Trovarelli, Catal. Rev.38 (1996) 439-520.
14. J.A. Dean, Lange's Handbook of Chemistry, 15th ed., McGraw-Hill Inc., New York, 1999, pp. 4.31-4.32.
15. S. Lee, H. Miyazaki, S.D. Mahanti, S.A. Solin, Phys. Rev. Lett.62 (1989) 3066-3069.
16. C.H. Ho, M.W. Ackerman, K.Y. Wu, T.N. Havill, R.H. Bogaard, R.A. Matula, S.G. Oh, H.M. James, J. Phys. Chem. Ref. Data 12 (1983) 231-232
17. D. Duprez, M.C. Demicheli, P. Marecot, J. Barbier, O. Ferretti, E.N. Ponzi, J. Catal. 124 (1990) 324-335.
18. C.H. Bartholomew, Catal. Rev. Sci. Eng. 24 (1982) 67-112.
19. J. Zhang, M. Safarzadeh, D.J. Young, Oxid. Met. 70 (2008) 15-24.
20. N.M. Galea, D. Knapp, T. Ziegler, J. Catal. 247 (2007) 20-33.
21. E. Nikolla, J.W. Schwank, S. Linic, Catal Today 136 (2008) 243-248.
22. E. Nikolla, J. Schwank, S. Linic, J. Catal. 250 (2007) 85-93.
23. M. Brown, S. Primdahl, M. Mogensen, J. Electrochem. Soc. 147 (2000) 475-485.